Selective Methanol-to-Formate Electrocatalytic Conversion on Branched Nickel Carbide

Junshan Li,[a] Ruilin Wei,[b] Xiang Wang,[c] Yong Zuo,[c] Xu Han,[d] Jordi Arbiol,[d,e] Jordi Llorca,[f] Yaoyue Yang,[b]* Andreu Cabot,[c,e]* Chunhua Cui[a]*

a Institute of Fundamental and Frontier Sciences, University of Electronic Science and Technology of China, 610054 Chengdu, P. R. China.

b College of Chemistry and Environmental Protection Engineering, Southwest Minzu University, 610041 Chengdu, P. R. China.

c Catalonia Institute for Energy Research - IREC, Sant Adrià de Besòs, Barcelona, 08930, Spain.

d Catalan Institute of Nanoscience and Nanotechnology (ICN2), CSIC and BIST, Campus UAB, Bellaterra, 08193 Barcelona, Spain.

e ICREA, Pg. Lluís Companys 23, 08010 Barcelona, Spain.

f Institute of Energy Technologies, Department of Chemical Engineering and Barcelona Research Center in Multiscale Science and Engineering. Universitat Politècnica de Catalunya, EEBE, 08019 Barcelona, Spain.

Abstract: We argue here that a methanol economy would be favored by the availability of low cost catalysts able to selective oxidize methanol to formate. A selective oxidation to formate would allow extracting the largest part of the fuel energy while simultaneously producing a chemical with even higher commercial value than the fuel itself. This reaction path would also reduce CO_2 emissions in direct methanol fuel cells and it would help to overcome the catalyst poisoning limitation which is related to a strong CO adsorption. However, a vital need to realize this scenario, is to screen out a reliable catalyst for the selective methanol oxidation reaction (MOR) and to determine the precise electrochemical conversion process, yet both of which remain unachieved. Here we present a highly active MOR catalyst based on abundant elements and with an optimized structure to simultaneously maximize interaction with the electrolyte and mobility of charge carriers. Using advanced *in-situ* infrared spectroscopy combined with the nuclear magnetic resonance, branched nickel carbide particles are the first catalyst determined to have nearly 100 % electrochemical conversion of methanol to formate without generating detectable CO_2 byproduct. Electrochemical kinetics analysis reveals the optimized reaction conditions and the electrode delivered an average current density up to 126.7 mA cm^{-2} in 1.0 M KOH, corresponding to a record value of 4.2 A mg^{-1} at 0.6 V *vs.* Ag/AgCl and a notable stability within 1000

continuous cycles. This work provides a straightforward and cost-efficient way for conversion of organic small molecules and the first direct evidence of a selective formate reaction path.

Keywords: branched particles; nickel carbide; *in-situ* infrared spectroscopy; methanol oxidation reaction; formic acid

Methanol is not only one of the most used commodity chemicals but also an excellent energy vector. Methanol is characterized by a high energy density (15.6 MJ/L), several times above that of liquid H_2 (4.7 MJ/L).[1] Being liquid at ambient temperature and pressure, methanol allows for an easy storing and transportation, and it could be distributed using the already existing infrastructure. Additionally, it can be renewably obtained from biomass, organic waste or CO_2.[2] All of these advantages, provide direct methanol fuel cells (DMFCs) with a high potential to power future electric cars and mobile applications, among others.[3] However, the massive depletion of DMFCs is currently impeded by the lack of active, durable and cost-effective catalysts, particularly for the methanol oxidation reaction (MOR).[4]

MOR is generally considered to proceed through a dual-pathway that involves either CO_{ad} or formate intermediates.[5] In the CO_{ad} path, the over-strong adsorption of CO poisons active catalytic sites limiting the catalyst durability. On the other hand, formate weakly bonds to the catalyst surface and it is easily dissolved in alkaline media. Thus, while the formate path does not allow the complete methanol oxidation, and therefore has associated lower energy densities (9.2 MJ/L), it may be preferred over the CO_{ad} path that rapidly blocks catalyst activity. An additional advantage of DMFCs based on a selective conversion of methanol to formate is the lack of CO_2 emissions during operation. On top of this, the production of a valuable chemical such as formate is advantageous in itself and it can reduce the overall fuel cost. Formate is actually an indispensable intermediate in the chemical industry due to its numerous applications in fabric dyeing, printing processes and the pharmaceutical industry.[6] Currently, close to one million tons of formic acid are yearly produced from the combination of methanol with CO at 40 atm and 80°C and the hydrolysis of the resulting methyl formate.[7] Owing to the high energy used in this process and the high demand, the price per metric ton of formate is a fourfold higher than that of methanol.[8,9] Therefore, the selective oxidation of methanol to formate in a DMFC can be even economically profitable if a proper strategy to collect the reaction product was developed.

The mechanism of methanol electrooxidation on Ru, Pd and Pt-based electrodes in alkaline and acid electrolytes has been extensively investigated.[5,10,11] These catalysts do not provide a selective conversion of methanol-to-formate and are too expensive and rare to empower the methanol economy. Among the several alternative materials proposed to replace noble metals as MOR catalysts, Ni offers the highest cost-effectiveness. A plethora of Ni[12–16] and Ni-based catalysts, including oxides/hydroxides,[17–22] metal alloys,[23–30] phosphides,[31] chalcogenides,[32] and nitrides,[33] have been

developed and tested toward MOR. Surprisingly, the nickel carbide, which a priori offers suitable properties as electrocatalysts, e.g. stability, electrical conductivity and element abundance, has not been tested toward MOR. On the other hand, while MOR mechanisms have been well-studied in noble metals, in spite of the high potential of Ni-based catalysts, their MOR pathways remain largely unknown.

In this work we propose a cost effective catalyst based on nickel carbide for the selective oxidation of methanol to formate. This highly selective oxidation allows extracting a significant part of the energy from the methanol molecules while at the same time transforming the fuel into a more valuable chemical. To demonstrate the MOR mechanism, we applied advanced *in-situ* and *ex-situ* characterization strategies combined with electrochemical kinetics analysis to identify the adsorbed and dissolved intermediates/products as a function of the applied potentials.

Ni_3C nanoparticles (NPs) were produced from the decomposition of nickel (II) acetylacetonate at 240 ºC in a solution of octadecene (ODE) and oleylamine (OAm).[34] Experimental details can be found on the supporting information (SI). Figure 1a displays a representative transmission electron microscopy (TEM) micrographs of the NPs produced using a solvent ratio ODE/OAm = 2. Particles produced under these conditions had an average size of 140±20 nm and appeared highly branched with an average branch width of 19±4 nm. When reducing the ODE/OAm ratio to 1, smaller particles, 53±7 nm, with shorter branches but with approximately the same width were produced (Figure S1). X-ray diffraction (XRD) patterns showed the crystallographic structure of the produced particles to match the rhombohedral Ni_3C_{1-x} phase (JCPDS 01 072 1467, Figure 1b).[35] High resolution TEM (HRTEM) characterization confirmed the crystallographic structure of the produced NPs to match the Ni_3C hexagonal phase (space group =R3-CH #167) with a=b=4.5820 Å and c=13.0300 Å.

X-ray photoelectron spectroscopy (XPS) data showed the probed Ni at the Ni_3C surface to have an oxidized $Ni^{2+/3+}$ chemical environment with Ni $2p_{3/2}$ at 857.1 eV (Figure S2).[36] This Ni_3C surface oxidation was attributed to the manipulation of the particles in air atmosphere during purification and transportation.[37,38]

Thermogravimetric analysis (TGA) of the Ni_3C NPs showed a weight loss of a 6.6 wt% when heating the material up to 450 ºC (Figure S3). This weight loss was associated to the desorption of surface water and the decomposition of the surface ligands used to control the NP growth. TGA showed

an additional weight loss of a 3.6wt% at temperature above 500 ºC, which was attributed to a carbon release from the structure, in agreement with previous reports.[34] To prepare the catalysts, the organic surface ligands were chemically removed using hydrazine and acetonitrile (see SI for details), and this removal was confirmed by FTIR analysis (Figure S4).

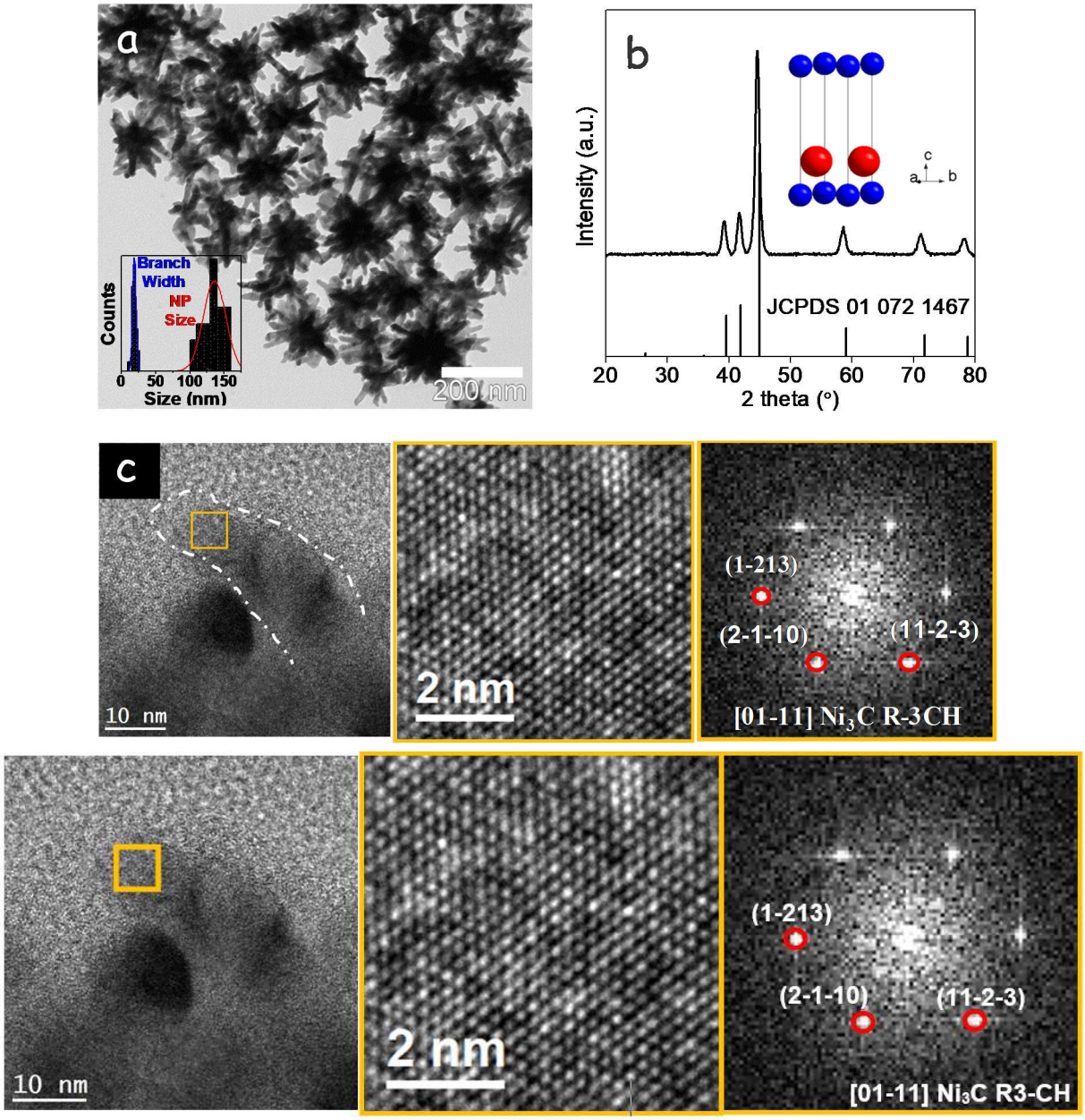

Figure 1. a) Representative TEM micrograph of the particles obtained within a solvent ration ODE/OAm=2. b) XRD pattern and Ni_3C crystal structure: blue = carbon, red = nickel. c) HRTEM micrograph, detail of the orange squared region and its corresponding power spectrum. From the displayed crystalline domain, lattice fringe distances were measured to be 0.203 nm, 0.234 nm, and 0.212 nm, at 60.45º and 127.18º, which was interpreted as a hexagonal Ni_3C phase visualized along its [01-11] zone axis.

Ni_3C-based electrocatalysts were prepared by drop-casting a solution containing the NPs and carbon black at a 1/2 weight ratio on top of glassy carbon (see SI for details). Initial cyclic voltammetry (CV) analysis of the electrocatalysts was performed in a 1.0 M KOH electrolyte (Figure 2a). During the forward scan, surface Ni was oxidized, first to $Ni(OH)_2$ and later to NiOOH.[25] Ni_3C/C electrodes activated the oxygen evolution reaction (OER) at ca. 0.6-0.7 V vs. Ag/AgCl and the lowest activation voltages were systematically measured with the larger and more branched Ni_3C NPs, i.e. those produced with ODE/OAm=2.

The electrochemically active surface area (ECSA) was estimated from the electrochemical double-layer capacitance (C_{dl}) on the basis of CVs recorded at different scan rates in the non-faradaic potential range 0-0.1 V vs. Ag/AgCl (see Figure S5 and calculations in SI for details).[39,40] An ECSA up to 65 cm^2 was obtained for the largest branched NPs and just 37.5 cm^2 for the smallest ones.

Figures 2b and S6ab display CVs with a stepwise increase of scanning rates from 10 to 150 mV s^{-1} in 1.0 M, 0.5 M and 0.1 M KOH. A continuous potential shift of the redox peaks was associated to the formation and diffusion of NiOOH species. From this data the surface coverage of Ni^{2+}/Ni^{3+} redox species (Γ^*) could be calculated by fitting a linear dependence of the redox peak current with the scanning rate (see Figures S6cd and S7a and calculations SI for details).[25] Figure 2c compares the coverage of redox species in different KOH concentrations obtained from this fitting for 0.1 M, 0.5 M and 1.0 M KOH (). Considering that the proton diffusion governs the $Ni^{2+} \Leftrightarrow Ni^{3+}$ redox reaction process, its diffusion coefficient (D) was determined by the *Randles-Sevcik* equation (see Figures S6efb and S7bef and calculations in SI).[41] The proton diffusion coefficients obtained in Ni_3C, up to 5.99×10^{-9} cm^2 s^{-1} in 1.0 M KOH (Figure 2c), were well above to the values measured for pure Ni NPs,[16] which indicates the N_3C structure to facilitate the Ni^{2+}/Ni^{3+} redox process at the basis of the high electrocatalytic activity of Ni-based catalysts.

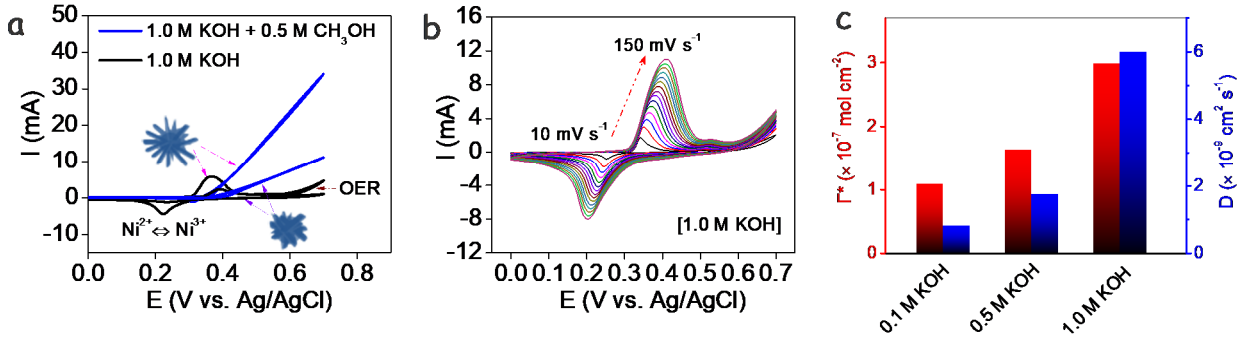

Figure 2. Electrochemical response of Ni_3C NPs in alkaline media. a) CV curves of N_3C NPs in 1.0 M KOH solution with and without 0.5 M methanol. b) CV curves in 1.0 M KOH at scanning rate from 10 mV s^{-1} to 150 mV s^{-1}. c) Surface coverage of redox species (Γ^*) and diffusion coefficient (D) obtained in 0.1, 0.5 and 1.0 M KOH solution.

Once methanol was added to the electrolyte, a sharp current density increase associated to the MOR was measured at potentials above 0.35 V, which matched well with the $Ni(OH)_2 \rightarrow NiOOH$ oxidation event (Figure 2a and 3a). As expected, current densities increased with the KOH concentration (Figure 3a), but also with the size and branching of the NPs (Figure 2a). When increasing the methanol concentration, the measured current density raised rapidly up to a 0.3 M methanol concentration and reached a plateau above 0.4 M (Figure 3b). To compare the MOR activity with reference materials, the oxidation current was normalized by the surface area or the Ni_3C mass loading. The current density at 0.6 V *vs.* Ag/AgCl in 1.0 M KOH and 1.0 M methanol reached 127 mA cm^{-2} and 4.2 A $mg_{Ni_3C}^{-1}$ (averaged from 5 separate electrodes with 10% error). These activities clearly stands out from previously reported noble metal-free MOR catalysts (Table S1). Discarding a bifunctional and a stearic effect of the carbon within the Ni, we associated the excellent catalytic activities obtained from nickel carbide-based catalysts to an electronic influence of the carbon on nickel-based surface reaction sites. Besides, we observed the unique branched geometry to booster the EOR activity by simultaneously providing a large electrolyte/electrode interface for methanol and hydroxide interaction with high electrical conductivity avenues for charge transport.

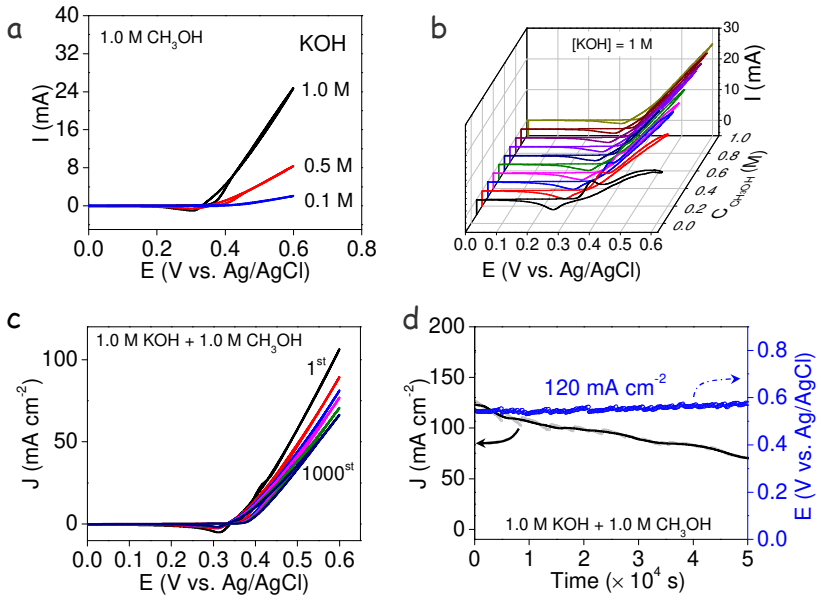

Figure 3. MOR electrochemical performance of Ni_3C-based electrodes. a) CV curves in 0.1, 0.5 and 1.0 M KOH solution with 1.0 M methanol. b) CV curves of highly branched N_3C NPs in 1.0 M KOH with

variable methanol concentrations from 0.1 to 1.0 M. c) Continuous CV cycling in the potential range 0-0.6V *vs.* Ag/AgCl with a scan rate of 100 mV s^{-1}. d) CA response at 0.6 V *vs.* Ag/AgCl and CP profile with at a current density of 120 mA cm^{-2}.

The electrochemical stability of Ni_3C electrocatalysts was evaluated through continuous CV cycling, chronoamperometry (CA) and chronopotentiometry (CP) in 1.0 M KOH and 1.0 M methanol. Figure 3c presents 1000 continuous CV cycles obtained from a branched Ni_3C/C catalyst. The current density at 0.6 V vs. Ag/AgCl was found to decay 18.1%, 24.4%, 28.6%, and 34.6% after the 200th, 600th, 800th and 1000th CV, respectively, but maintaining still 69.6 mA cm^{-2} after 1000 cycles. Figure 3d shows the CA curve at 0.6 V, where an insignificant OER contribution was measured (Figure 2a). In these conditions, as shown in Figure 3d, during 5000 s operation the current density decreased from 125 mA cm^{-2} to 70 mA cm^{-2}, which is still an excellent current density if we compare with initial values reported in previous works (Table S1). Additionally, CP measurements showed that an additional potential of just 0.03 V, on top of the initial 0.55 V, were required to maintain a current density of 120 mA cm^{-2} for 50,000 s (Figure 3d).

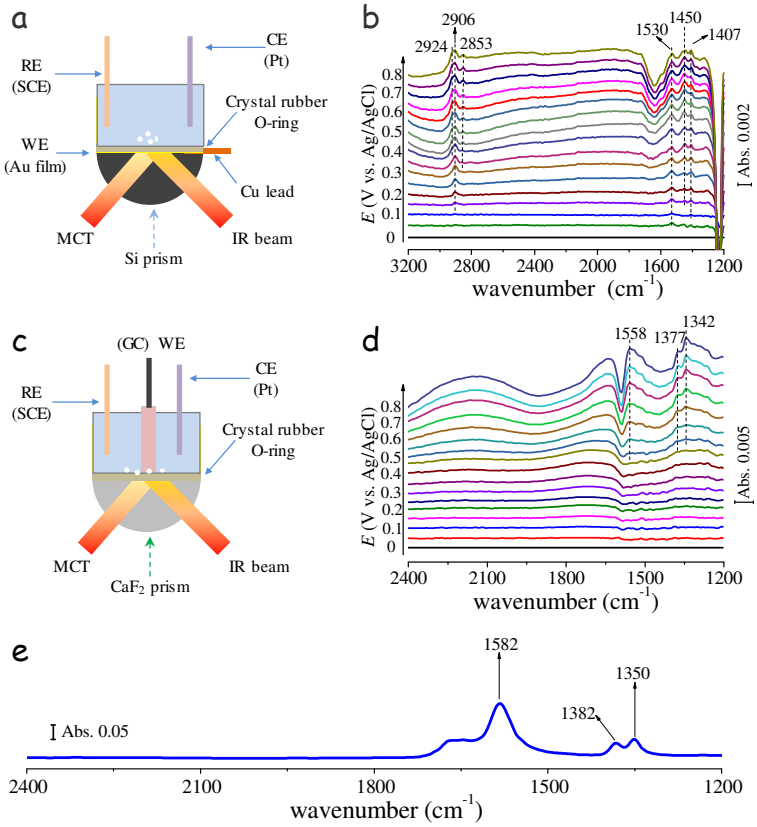

Figure 4. a) Schematic drawing of the ATR-SEIRA set-up. b) Real-time ATR-SEIRA spectra taken on branched Ni_3C surface in 0.1 M KOH and 0.5 M methanol in the potential range 0-0.8 V *vs.* Ag/AgCl. c) Schematic drawing of a typical setup for IRAS. d) Real-time spectra of MOR on branched Ni_3C NPs

surface in 0.1 M KOH and 0.5 M methanol in the potential range 0-0.8 V *vs.* Ag/AgCl. e) Transmission spectra of 0.05 M HCOONa and 0.1 M KOH. Note The single-beam spectrum collected at 0 V was used as the reference spectrum of the real-time spectra, and spectral resolution is 8 cm^{-1}.

To determine the MOR reaction mechanism and the reason behind the excellent catalyst stability, we monitored the MOR activity of Ni_3C-based electrodes using *in-situ* Attenuated Total Reflection Surface-Enhanced Infrared Absorption (ATR-SEIRA) and Infrared Reflection Absorption Spectroscopy (IRAS) in a 0.1 M KOH electrolyte containing 0.5 M methanol. To the best of our knowledge *in situ* infrared spectroscopy has not been used previously to analyze the MOR mechanism in Ni-based non noble-metal electrocatalyts. As shown in Figure 4a, several IR absorption peaks appeared in the ATR-SEIRA spectra when applying potentials above 0.2 V *vs.* Ag/AgCl to the Ni_3C electrode. Specifically, IR absorption bands at ca. 2924, 2906 and 2853 cm^{-1} as well as three peaks at 1530, 1540, and 1407 cm^{-1} in the lower wavenumber region are ascribed to surface CH_3O and CH_3OH species (see Table 1).[10,42–45] Notably, no evidences were found of the presence of neither adsorbed CO species (1700-2000 cm^{-1}) nor of the CO_2 production (2341 cm^{-1}) in the ATR-SEIRA spectra. Nevertheless, the presence of these species cannot be excluded only based on ATR-SEIRA spectra, as weakly-adsorbed or produced species may dissolve into the solution. Thus, we used IRAS to analyze at each electrode potential the dissolved products in a thin electrolyte layer used in this experiment (see setup drawing in Figure 4c). As shown in Figure 4d, no bands associated with CO and CO_2 could be observed, which excluded the CO-pathway in the MOR on Ni_3C. On the other hand, bands at ca.1558, 1377 and 1342 cm^{-1} in the IRAS spectra were assigned to formate (Figure 4e and Table 1).[42,46] Note that the peak at 1588 cm^{-1} should be located at ca. 1580 cm^{-1}, but the slight shift observed can be associated to the overlap with the (HOH) band of interfacial water (1630 cm^{-1} downward) present during the methanol consumption on the NPs surface. Additionally, IRAS spectra showed no sign of the presence of CO_2 or carbonate at higher potential, which pointed at formate as the only product of the MOR at the Ni_3C surface. Figure S8 displays the intensity of the band at 1342 cm^{-1} as a function of the applied potential during a typical CV in 0.1 M KOH with 0.5 M methanol. A clear relationship between the current density onset associated to the MOR and the band corresponding to the presence of formate in solution was observed.

Table 1. Band assignments from the ATR-SEIR and IRAS spectra displayed in figure 4

wavenumber / cm^{-1}	assignments
2924, 2853	ν(C-H) of CH_3OH or CH_3O[10,42,43]
2907	$\delta_{as}(CH_3)$ of CH_3OH or CH_3O[42]

1530, 1450	δ(C-H) of CH_3OH or CH_3O[10,42,43]
1407	CO_3^{2-} or -COOH[44,45]
1558	ν_{as}(OCO) of HCOO-[42,46]
1377	δ(C-H) of HCOO-[46]
1342	ν_s(OCO) of HCOO-[46]

To validate our results, an aliquot of the electrolyte after MOR operation in 1.0 M KOH + 1.0 M methanol was analyzed by NMR (Figure S9). ^{13}C NMR analysis indicated that the formate was the only product after 50000 s reaction, further demonstrating the highly selective conversion of methanol to formate over Ni_3C catalysts in alkaline media.

In summary, we presented a new MOR catalyst based on abundant elements able to selectively and effectively convert methanol-to-formate. We demonstrated that branching the catalyst particles strongly enhanced their performance. Electrochemical measurements combined with advanced *in-situ* infrared spectroscopy and NMR analysis allowed to clearly determine the reaction products ruling out the adsorption of CO and the production of carbonates. This highly selective conversion on Ni_3C electrodes exhibited a remarkable current density of 126.7 mA cm^{-2}, corresponding to 4.2 A mg^{-1} at 0.6 V *vs.* Ag/AgCl in 1.0 M KOH containing 1.0 M methanol. This work offers first evidence for this selective methanol-to-formate conversion in Ni-based catalysts and provides a very promising example to exploit non-precious metal oxides for the electrocatalytic conversion of small organic molecules.

Author Information

Corresponding Author

* Prof. Yaoyue Yang: yaoyueyoung@swun.edu.cn

* Prof. Andreu Cabot: acabot@irec.cat

* Prof. Chunhua Cui: chunhua.cui@uestc.edu.cn

Author contributions

The manuscript was prepared through the contribution of all authors. C. Cui and A. Cabot conceived and guided the project, and supervised the work. J. Li designed the experiments, produced the NPs, conducted XRD, TEM and FT-IR characterization, electrochemical measurements, and wrote the first draft. X. Wang and Y. Zuo significantly contributed to the results discussion. R. Wei and Y. Yang

performed the *in-situ* infrared spectroscopic measurements and discussed the data. X. Han and J. Arbiol conducted structural and compositional NPs characterization by means of HRTEM and EELS, and discussed the results. J. Llorca measured and discussed XPS data. The manuscript was corrected and improved by all authors.

Acknowledgements

This work was supported from the UESTC start-up funding and the Recruitment Program of Thousand Youth Talents. J. Li obtained *International Postdoctoral Exchange Fellowship Program (Talent-Introduction program)* in 2019 and is grateful for the project (2019M663468) funded by the China Postdoctoral Science Foundation. This work was also supported by the European Regional Development Funds and by the Spanish Ministerio de Economía y Competitividad through the project SEHTOP (ENE2016-77798-C4-3-R) and VALPEC (ENE2017-85087-C3). X. wang, Y. Zuo, and X. Han thank the China Scholarship Council (CSC) for scholarship support. J. Arbiol and X. Han acknowledge funding from Generalitat de Catalunya 2017 SGR 327. ICN2 acknowledges support from the Severo Ochoa Programme (MINECO, Grant no. SEV-2013-0295). IREC and ICN2 are funded by the CERCA Programme / Generalitat de Catalunya. Part of the present work has been performed in the framework of Universitat Autònoma de Barcelona Materials Science PhD program. J. Llorca is a Serra Húnter Fellow and is grateful to MICINN/FEDER RTI2018-093996-B-C31, GC 2017 SGR 128 and to ICREA Academia program.

Conflict of interest

The authors declare no competing financial interest.

Reference

[1] A. Sartbaeva, V. L. Kuznetsov, S. A. Wells, P. P. Edwards, *Energy Environ. Sci.* **2008**, *1*, 79–85.
[2] N. Kakati, J. Maiti, S. H. Lee, S. H. Jee, B. Viswanathan, Y. S. Yoon, *Chem. Rev.* **2014**, *114*, 12397–12429.
[3] S. P. S. Badwal, S. Giddey, A. Kulkarni, J. Goel, S. Basu, *Appl. Energy* **2015**, *145*, 80–103.
[4] X. Zhao, M. Yin, L. Ma, L. Liang, C. Liu, J. Liao, T. Lu, W. Xing, *Energy Environ. Sci.* **2011**, *4*, 2736.
[5] E. Herrero, W. Chrzanowski, A. Wieckowski, *J. Phys. Chem.* **1995**, *99*, 10423–10424.
[6] H. Robles, in *Encycl. Toxicol.*, Wiley-VCH Verlag GmbH & Co. KGaA, Weinheim, Germany, **2005**, pp. 378–380.
[7] Q. Liu, L. Wu, S. Gülak, N. Rockstroh, R. Jackstell, M. Beller, *Angew. Chemie - Int. Ed.* **2014**,

53, 7085–7088.

[8] M. Li, X. Deng, K. Xiang, Y. Liang, B. Zhao, J. Hao, J. L. Luo, X. Z. Fu, *ChemSusChem* **2019**, *13*, 914–921.

[9] J. Eppinger, K. W. Huang, *ACS Energy Lett.* **2017**, *2*, 188–195.

[10] Y. Y. Yang, J. Ren, H. X. Zhang, Z. Y. Zhou, S. G. Sun, W. Bin Cai, *Langmuir* **2013**, *29*, 1709–1716.

[11] W. Huang, H. Wang, J. Zhou, J. Wang, P. N. Duchesne, D. Muir, P. Zhang, N. Han, F. Zhao, M. Zeng, et al., *Nat. Commun.* **2015**, *6*, 10035.

[12] R. M. Abdel Hameed, R. M. El-Sherif, *Appl. Catal. B Environ.* **2015**, *162*, 217–226.

[13] S. Das, K. Dutta, P. P. Kundu, *J. Mater. Chem. A* **2015**, *3*, 11349–11357.

[14] H. Sun, Y. Ye, J. Liu, Z. Tian, Y. Cai, P. Li, C. Liang, *Chem. Commun.* **2018**, *54*, 1563–1566.

[15] S. Xie, X.-L. Tong, G.-Q. Jin, Y. Qin, X.-Y. Guo, *J. Mater. Chem. A* **2013**, *1*, 2104–2109.

[16] J. Li, Y. Zuo, J. Liu, X. Wang, X. Yu, R. Du, T. Zhang, M. F. Infante-Carrió, P. Tang, J. Arbiol, et al., *J. Mater. Chem. A* **2019**, *7*, 22036–22043.

[17] L. Wang, G. Zhang, Y. Liu, W. Li, W. Lu, H. Huang, *Nanoscale* **2016**, *8*, 11256–11263.

[18] X. Tong, Y. Qin, X. Guo, O. Moutanabbir, X. Ao, E. Pippel, L. Zhang, M. Knez, *Small* **2012**, *8*, 3390–3395.

[19] M. Asgari, M. G. Maragheh, R. Davarkhah, E. Lohrasbi, *J. Electrochem. Soc.* **2011**, *158*, K225.

[20] T. Wang, H. Huang, X.-R. Wu, H.-C. Yao, F. Li, P. Chen, P. Jin, Z. Deng, Y. Chen, *Nanoscale* **2019**, DOI 10.1039/c9nr06304h.

[21] J. Wang, D. Teschner, Y. Yao, X. Huang, M. Willinger, L. Shao, R. Schlögl, *J. Mater. Chem. A* **2017**, *5*, 9946–9951.

[22] S. Rezaee, S. Shahrokhian, *Appl. Catal. B Environ.* **2019**, 802–813.

[23] J. Li, Z. Luo, Y. Zuo, J. Liu, T. Zhang, P. Tang, J. Arbiol, J. Llorca, A. Cabot, *Appl. Catal. B Environ.* **2018**, *234*, 10–18.

[24] J. Li, Z. Luo, F. He, Y. Zuo, C. Zhang, J. Liu, R. Du, X. Yu, T. Zhang, P. Tang, et al., *J. Mater. Chem. A* **2018**, *6*, 22915–22924.

[25] X. Cui, P. Xiao, J. Wang, M. Zhou, W. Guo, Y. Yang, Y. He, Z. Wang, Y. Yang, Y. Zhang, et al., *Angew. Chemie - Int. Ed.* **2017**, *56*, 4488–4493.

[26] D. Wu, W. Zhang, D. Cheng, *ACS Appl. Mater. Interfaces* **2017**, *9*, 19843–19851.

[27] I. S. Pieta, A. Rathi, P. Pieta, R. Nowakowski, M. Hołdynski, M. Pisarek, A. Kaminska, M. B. Gawande, R. Zboril, *Appl. Catal. B Environ.* **2019**, *244*, 272–283.

[28] R. Ding, J. Liu, J. Jiang, F. Wu, J. Zhu, X. Huang, *Catal. Sci. Technol.* **2011**, *1*, 1406–1411.

[29] X. Cui, W. Guo, M. Zhou, Y. Yang, Y. Li, P. Xiao, Y. Zhang, X. Zhang, *ACS Appl. Mater. Interfaces* **2015**, *7*, 493–503.

[30] S. L. Candelaria, N. M. Bedford, T. J. Woehl, N. S. Rentz, A. R. Showalter, S. Pylypenko, B. A. Bunker, S. Lee, B. Reinhart, Y. Ren, et al., *ACS Catal.* **2017**, *7*, 365–379.

[31] Y. Y. Tong, C. D. Gu, J. L. Zhang, M. L. Huang, H. Tang, X. L. Wang, J. P. Tu, *J. Mater. Chem. A* **2015**, *3*, 4669–4678.

[32] Q. Luo, M. Peng, X. Sun, A. M. Asiri, *RSC Adv.* **2015**, *5*, 87051–87054.

[33] M. Mazloum-Ardakani, V. Eslami, A. Khoshroo, *Mater. Sci. Eng. B Solid-State Mater. Adv. Technol.* **2018**, *229*, 201–205.

[34] Z. L. Schaefer, K. M. Weeber, R. Misra, P. Schiffer, R. E. Schaak, *Chem. Mater.* **2011**, *23*, 2475–2480.

[35] L. Qiao, W. Zhao, Y. Qin, M. T. Swihart, *Angew. Chemie Int. Ed.* **2016**, *55*, 8023–8026.

[36] W. C.D., R. W.M., D. L.E., M. J.F., *Handbook of X-Ray Photoelectron Spectroscopy*, Perkin-Elmer Corporation Physical Electronics Division, Minnesota, **1979**.

[37] J. Li, X. Xu, Z. Luo, C. Zhang, Y. Zuo, T. Zhang, P. Tang, M. F. Infante-Carrió, J. Arbiol, J. Llorca, et al., *ChemSusChem* **2019**, *12*, 1451–1458.

[38] J. Li, X. Xu, X. Yu, X. Han, T. Zhang, Y. Zuo, C. Zhang, D. Yang, X. Wang, Z. Luo, et al., *ACS Appl. Mater. Interfaces* **2020**, *12*, 4414–4422.

[39] J. D. Benck, Z. Chen, L. Y. Kuritzky, A. J. Forman, T. F. Jaramillo, *ACS Catal.* **2012**, *2*, 1916–1923.

[40] C. C. L. McCrory, S. Jung, I. M. Ferrer, S. M. Chatman, J. C. Peters, T. F. Jaramillo, *J. Am. Chem. Soc.* **2015**, *137*, 4347–4357.

[41] A. J. Bard, L. R. Faulkner, *Electrochemical Methods: Fundamentals and Applications*, **2001**, Chapter 4, 137-155.

[42] S. E. Collins, M. A. Baltanás, A. L. Bonivardi, *Appl. Catal. A Gen.* **2005**, *295*, 126–133.

[43] Y. Liu, M. Muraoka, S. Mitsushima, K. I. Ota, N. Kamiya, *Electrochim. Acta* **2007**, *52*, 5781–5788.

[44] A. Zalineeva, S. Baranton, C. Coutanceau, *Electrochim. Acta* **2015**, *176*, 705–717.

[45] Y. Zhu, H. Uchida, T. Yajima, M. Watanabe, *Langmuir* **2001**, *17*, 146–154.

[46] A. Kowal, S. N. Port, R. J. Nichols, *Catal. Today* **1997**, *38*, 483–492.